




## Article

# Rockfall Threatening Cumae Archeological Site Fruition (Phlegraean Fields Park—Naples)

Rita De Stefano <sup>1</sup>, Leopoldo Repola <sup>2</sup>, Luigi Guerriero <sup>1,\*</sup>, Domenico Iovane <sup>3</sup>, Vincenzo Morra <sup>1</sup>, Fabio Pagano <sup>4</sup> and Diego Di Martire <sup>1</sup>

- <sup>1</sup> Monte Sant' Angelo Campus, Department of Earth Sciences, Environment and Resources, Federico II University of Naples, 21, Cinthia Street, 80126 Naples, Italy; rita.destefano@unina.it (R.D.S.); vincenzo.morra@unina.it (V.M.); diego.dimartire@unina.it (D.D.M.)
- <sup>2</sup> Department of Humanities, Suor Orsola Benincasa University, 10, Suor Orsola Street, 80135 Naples, Italy; repolaleopoldo@gmail.com
- <sup>3</sup> Department of Architecture, Federico II University of Naples, 36, Forno Vecchio Street, 80134 Naples, Italy; domenico.iovane@unina.it
- <sup>4</sup> Phlegraean Fields Archeological Park, Rione Terra, Palazzo De Fraja, 80078 Pozzuoli, Italy; fabio.pagano@beniculturali.it
- \* Correspondence: luigi.guerriero2@unina.it

**Abstract:** Natural hazards threaten many archaeological sites in the world; therefore, susceptibility analysis is essential to reduce their impacts and support site fruition by visitors. In this paper, rockfall susceptibility analysis of the western slope of the Cumae Mount in the Cumae Archaeological Site (Phlegraean Fields, Naples), already affected by rockfall events, is described as support to a management plan for fruition and site conservation. Being the first Greek settlement in southern Italy, the site has great historical importance and offers unique historical elements such as the Cumaean Sibyl's Cave. The analysis began with a 3D modeling of the slope through digital terrestrial photogrammetry, which forms a basis for a geomechanical analysis. Digital discontinuity measurements and cluster analysis provide data for kinematic analysis, which pointed out the planar, wedge and toppling failure potential. Subsequently, a propagation-based susceptibility analysis was completed into a GIS environment: it shows that most of the western sector of the site is susceptible to rockfall, including the access course, a segment of the Cumana Railroad and its local station. The work highlights the need for specific mitigation measures to increase visitor safety and the efficacy of field-based digital reconstruction to support susceptibility analysis in rockfall prone areas.

**Keywords:** rockfall; cultural heritage fruition; photogrammetry; kinematic analysis; geomechanical analysis; Phlegraean Fields



**Citation:** De Stefano, R.; Repola, L.; Guerriero, L.; Iovane, D.; Morra, V.; Pagano, F.; Di Martire, D. Rockfall Threatening Cumae Archeological Site Fruition (Phlegraean Fields Park—Naples). *Sustainability* **2021**, *13*, 1390. <https://doi.org/10.3390/su13031390>

Academic Editor: Simone Mineo  
Received: 23 December 2020  
Accepted: 26 January 2021  
Published: 29 January 2021

**Publisher's Note:** MDPI stays neutral with regard to jurisdictional claims in published maps and institutional affiliations.



**Copyright:** © 2021 by the authors. Licensee MDPI, Basel, Switzerland. This article is an open access article distributed under the terms and conditions of the Creative Commons Attribution (CC BY) license (<https://creativecommons.org/licenses/by/4.0/>).

## 1. Introduction

The province of Naples is known for its cultural heritage, expression of the city's and its surrounding zones' history. It is rich in archaeological sites and parks that have preserved its historic asset and that have been increasingly exploited by means of specific projects and adoption of measures aimed at improving sites and making their fruition safer [1,2]. The Santa Chiara Site, the Posillipo and the Cumae Archaeological sites are only a few examples of the great cultural value sites. Specifically, the Cumae Archaeological Site (Figure 1) [3–5], in the Phlegraean Fields Park, harbors the homonymous ancient city. Being the first Greek western colony, founded in the second half of the 8th century B.C., Cumae is one of the most important archaeological sites of the area. Divided into the upper and lower city, it includes a variety of elements like the Greek walls of the late fifth century B.C., the ruins of the Temple of Apollo, of the Temple of Jupiter, the Roman crypt, the thermal baths, the Amphitheater and the Forum. The archaeological site is also known for the Cumaean Sibyl's Cave [5], one of the most famous oracles of the ancient world (Figure 1).

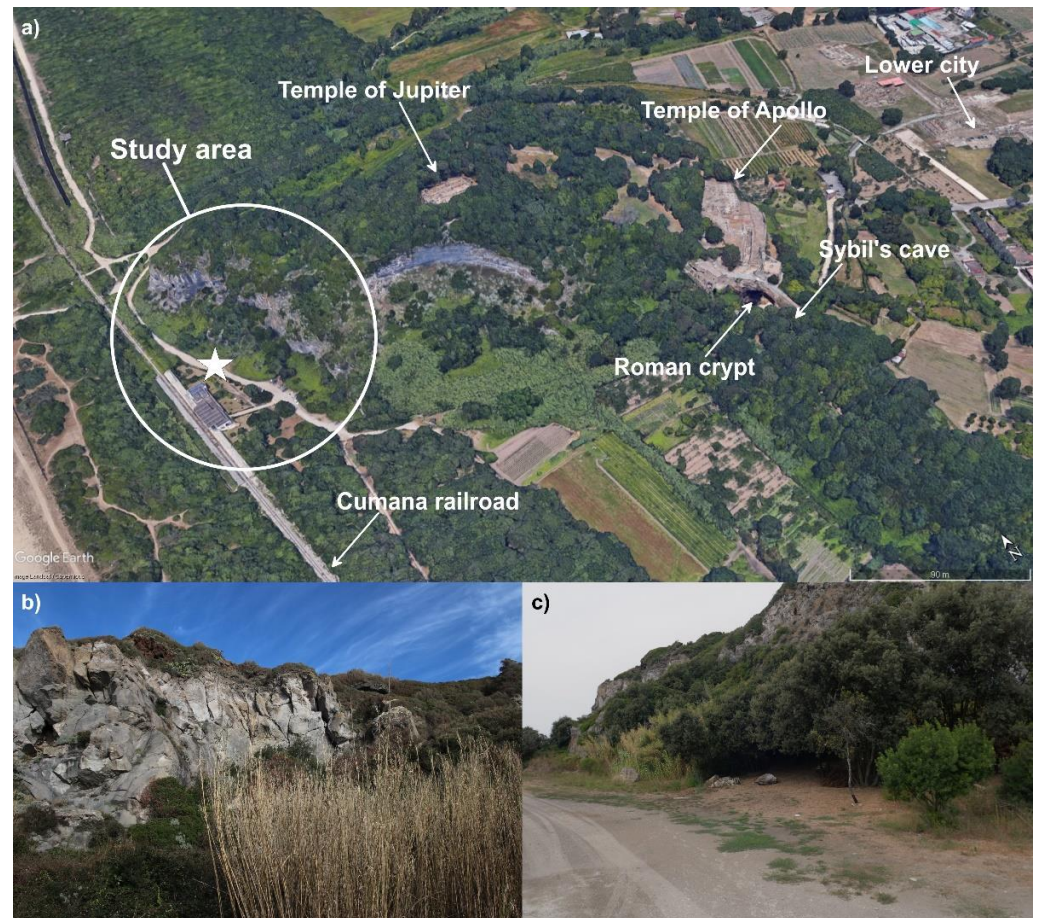


**Figure 1.** (a) Cumae Archaeological Site as seen from Google Earth model. Artworks indicate the study area and major elements of the site. The white star indicates the location of the rockfall event in 2009. (b) Northern sector of the front object of the study; (c) remnant of past rockfall event occurred in August 2019.

The Phlegraean Fields area is known for its exposure to landslide hazards, e.g., [6–9]. Indeed, the widespread presence of unconsolidated pyroclastic deposits, associated with both hard and weak volcanic rocks, predisposes slopes to fast-moving landslides [10–15]. While debris flows and avalanches, triggered by rainfall, are very common in the presence of steep slopes covered by pyroclastic soils, rock-slope instabilities, like rockfall and topples, are common in the presence of vertical, highly fractured tuff and lava cliffs [16]. As a consequence, at the Camaldoli Hill (i.e., the highest peak of the Phlegraean Fields area, 458 m asl), vertical or subvertical cliffs formed by lithified materials are frequently affected by rockfall and block size is consistently controlled by the main discontinuity systems in the rock mass. Additional events have been registered at the Cumae Mount that, in this perspective, represents a hotspot. Indeed, in the last decades, highly fractured material forming the lava dome (Figure 1b) has been consistently affected by rockfall hitting the access course to the site, the Cumana Railroad and the related station that supports visitors transfer to the site, with important implications for visitor safety. A recent event occurred in August 2019 when a 0.5 m<sup>3</sup> boulder detached from the northern slope of the Cumae Mount and reached the access course immediately downslope, halting not far from the Cumana Railroad (Figure 1c). As a result, because of the persisting presence of people in that part of the site, the Cumae Archeological Site was closed with important economic loss.

In the occurrence of rockfall events, a susceptibility analysis is always recommended in order to localize critical conditions and define zonation, which is the first step to risk analysis and adoption of mitigation measurements and plans [17]. As pointed out by Corominas et al. [17], landslide susceptibility can be assessed by means of either quali-

tative or quantitative methods. Qualitative analyses are mostly based on expertise, and susceptibility maps can be prepared on the basis of geomorphologic field interpretations. Quantitative analyses can be completed using data-driven statistical methods or physically based methods. Rockfall susceptibility is often assessed using quantitative approaches. Although hybrid statistical/physically-based approaches have been successfully adopted, GIS-based statistical analyses are often preferred over large areas [18–21]. Differently, slope-scale analyses are mostly completed using discontinuity analyses associated with physically based propagation models [22]. Recent developments in terrestrial laser scanning and photogrammetry can support discontinuity analysis and have been increasingly used in rockfall analyses [23–26]. Such methods are also commonly used in archaeological site analysis and restoration; moreover, in case of landslides affecting cultural heritage sites [27,28], they are of great importance to process understanding, potential-damage mitigation and increase visitor safety.

A photogrammetry-based analysis of the susceptibility to rockfall of the southern slope of Cumae Mount has been accomplished. The aim of this paper is to provide new insights into rockfall susceptibility, which may guide mitigation and assessment-plan development for safer fruition of the Cumae Archeological Site by visitors. For this purpose, field analyses supported by high-resolution terrestrial photogrammetric surveys were carried out in order to improve the susceptibility analysis, implemented by means of the QPROTO plugin [29], which considers detachment, propagation and deposition of the rock masses.

## 2. The Cumae Archeological Site

### 2.1. Historic and Archaeological Features

The Cumae site is located a few kilometers north of Naples, and it has been inhabited over a 2000-year period. Excavation works carried out in this area have brought to light substantial traces of the first phase of Greek colonization (mid-eighth century B.C.) after a previous occupation by local people (shown by burial sites). The city reflects the Greek model of urban design and social articulation. It consists of a fortified acropolis, of the lower city and of a vast surrounding territory. Between the eighth and seventh centuries B.C., it experienced an intense political and economic development that reached its height at the end of the sixth century B.C. under the tyranny of Aristodemus. After a period of occupation by the Samnites (421 B.C.), the city became part of the Roman world (334 B.C.). In this period, the image of the city was completely redesigned: the main public spaces and places of worship were monumentalized, and its memory was carved into the pages of the Aeneid, Book VI.

From the end of the third century A.D., transformation processes began, leading to the abandonment of the lower city, also due to marshes, and to the military occupation of the acropolis, which kept on existing as a castrum (army camp) until 1207. The stratified history of the town takes the material forms of an articulated set of fragments and architectural models. The upper terrace of the acropolis was dominated by the presence of two large temples, which, according to recent interpretations, could be attributed to the cult of Apollo (Figure 2a) and Jupiter (Figure 2b). A base in “opera isodoma” traced back the construction phases to the sixth century B.C., while the cementitious structures, with opus reticulatum cover, suggest that the temple reconstruction took place in the Roman age and was later transformed into a church. The same succession of phases can be found in the sanctuary located on the lower terrace, scenically leaning on the lower city and flanked by the fortifications built with tuff blocks, dating back to the sixth century B.C. It was adapted during the Greek-Gothic war to convert the acropolis into a castrum. A similar stratification can also be found in the negative architectures, such as the so-called Cumaean Sybil’s Cave (Figure 2c), where a trapezoidal-shape, the military tunnel was excavated during the Samnite age, reshaped in the Roman age and later transformed in a place of worship and a burial site during the Christian period. The monumental aspect of the city in Roman times (Figure 2d), which found its full definition during the Augustan age, can

be thoroughly perceived in the lower city, especially in the area where the Forum was established, probably overlapping the Greek Agora.



**Figure 2.** Major archeological elements of the Cumae archeological Site: (a) upper terrace temple; (b) lower terrace temple; (c) Cumaean Sybil's Cave; (d) Roman crypt; (e) Capitulum at the lower city.

In the third century B.C., a large uncovered rectangular square was modeled and paved with limestone slabs. It was surrounded by a portico (early 1st century B.C.) supported by Doric columns on the first level and Ionic columns on the second one and adorned with friezes of arms and masks in gray tuff relief. The short side of the Forum was dominated by the greatness of Capitulum (Figure 2e), a huge temple on a podium with a tripartite cell that overlaps a previous temple dating back to the 4th century B.C. The opposite side of the square was marked by the presence of the so-called “Tempio del Gigante” (mid-1st century A.D.) with a vaulted cell placed on a high podium, in the center of an open courtyard surrounded on three sides by arcades. It defined a space entirely covered in marble with a monumental façade overlooking the access road to the Forum.

## 2.2. Geological Context

The Cumae Archeological Site is located in the western part of the Neapolitan volcanic district inside the Campanian Plain, a vast, flat area on the Tyrrhenian edge of the southern Apennines. The geological features of the area, which are related to the activity of this active volcanic field [9], are shown in Figure 3. Its last eruptive event was the historic eruption of Monte Nuovo (1538 AD) [30] occurred after a period of quiescence of about 3000 years. Additional eruptions are known for their magnitude and their predominant explosive nature. The most powerful eruptions produced the Ignimbrite Campana (CI; ~39 ka) [31,32] and the Neapolitan Yellow Tuff (NYT; ~15 ka) [33], which are widespread throughout the province of Naples. These are the most important events of the volcanic history of the area: they determined the development of the Phlegraean Fields nested caldera [34]. In this framework, the deposits of CI and NYT are relevant chronostratigraphic markers in the reconstruction of the Phlegraean activity, which can be approximately divided into (1) pre-CI period, (2) between CI and NYT period, and (3) post-NYT period [34]. Moreover, due to the volcanic activity of the Phlegraean Fields, a diffuse cover of pyroclastic deposits associated with isolated domes and lava flows [35] has been formed. Currently, the Phlegraean Fields are experiencing a period of quiescence, showing its magmatism through seismicity and relatively benign hydrothermal and fumaroles' events.

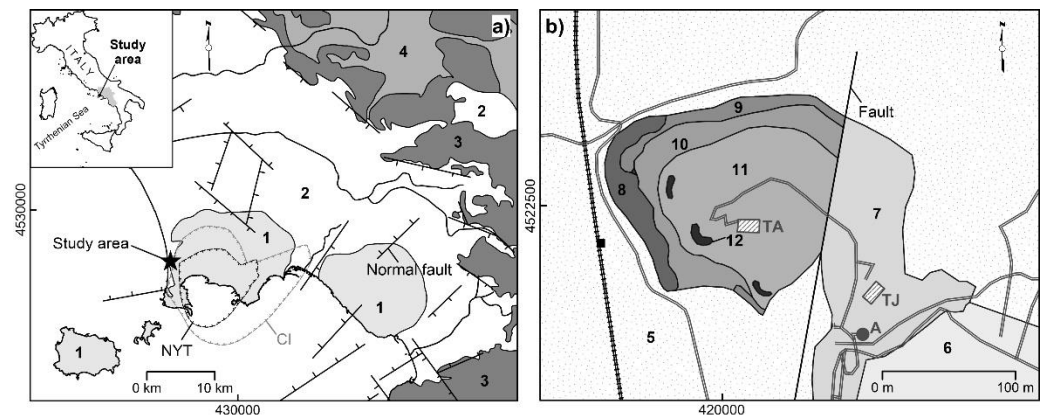


**Figure 3.** (a) Geological map of the area surrounding the Cumae Archeological Site (modified from [36]). Legend: (1) Quaternary epiclastic deposits; (2) Quaternary volcanic deposits; (3) Apennine platform carbonates; (4) Miocene deposits. The NYT caldera boundary and the CI caldera boundary are labeled as well as normal faults and the study area; (b) geological sketch map of the Cumae Archeological Site (modified from [37]). Legend: (5) eluvial-colluvial deposits; (6) pyroclastic deposits; (7) Neapolitan yellow tuff; (8) lava deposits of the Cumae Mount Formation; (9) slag deposits of the Cumae Mount Formation; (10) slope deposits; (11) pyroclastic deposits of the Cumae Mount Formation; (12) pumiceous pyroclastic deposits of the Breccia Museo Formation; Temple of Apollo (TA); Temple of Jupiter (TJ); Roman crypt (A) are shown. Major roads are reported. In both maps, UTM 33 N coordinates are reported at maps' edges.

### 2.3. Geological Setting of the Site

The Cumae Archeological Site is located along the western edge of the caldera of the Phlegraean Fields, whose sectors are characterized by several normal buried faults, fractures and deep crater circles [38,39]. The Cumae Archeological Site consists of a lower town and of an upper town. The lower city is mainly made up of Neapolitan Yellow Tuff, with a different degree of lithification. At the entrance of the Roman crypt, the deposit is semi-coherent with little altered pumices, while at the entrance of the Acropolis of Cumae, it is essentially lithoid and has columnar cracks. The lower city and the upper city are divided by the edge of the calderic collapse of the CI eruption. The Cumae Mount hosts the upper city, which is characterized in the northern sector by pyroclastic deposits [37], sometimes alternating with thin layers of ash. Such deposits are divided into two units [37]: a basal one, called *scoriae a*), consisting of layers of red slag with sharp edges alternating with layers of coarse ash and lava fragments, and the upper part, named *scoriae b*), characterized by juvenile slag fragments of centimetric and metric dimensions, collapsed and plastically deformed. *Scoriae b*) is extremely welded in the northern slope of Cumae Mount. The south-southeast portion of Cumae Mount is characterized by compact, intensely fractured trachifonolytic lava [35] (Figure 1b), covered by slag and lava blocks originated from the CI eruption and reaching 1 m thickness. This sector is particularly fractured and has been affected by important rockfall phenomena (Figure 1c). On this basis and considering the object of the analysis, zoning of the rock face in terms of fracturing degree can be observed.

## 3. Materials and Methods

The susceptibility to rockfall of the western slope of the Cumae Mount was analyzed using a GIS-based approach supported by a geomechanical and structural analysis of a dense point cloud derived from a ground-based photogrammetric survey.

### 3.1. Photogrammetric Survey

A terrestrial photogrammetric survey was carried out in order to reconstruct the 3D model of the western slope of the Cumae Mount. Geo-mechanical and structural

analyses were carried out by means of ShapeMetriX 3D (©3GSM GmbH) software using structure from motion approach (SfM). SfM is a method of photogrammetry that allows the reconstruction of high-resolution 3D models using multiple images without needing to set ground control points. Digital photogrammetry has been applied to a number of geological problems, including discontinuity characterization [40,41] and rock slope stability analysis [42–44]. This approach was chosen because it is able to perform analyses on the basis of slope-morphological features and of the limited presence of vegetation.

It is well known that the photogrammetric technique allows reconstructing objects in the form of three-dimensional point clouds starting from two-dimensional image sets [45,46]. In order to obtain uniform coverage of the area, it is necessary, during the acquisition phase, to maximize the overlap by adopting short baselines. For this work, a calibrated Canon EOS 80D camera equipped with a lens characterized by a focal length of 17.14 mm was used. Pictures were taken using a tripod, keeping a consistent orientation of the camera and a 1.50 m height from the ground. A total of 164 frames were acquired considering a normal distance of 30 m from the front and one longitudinal acquisition step of 1 m. In this way, an approximately 80% overlap was reached. In order to maximize model quality, the acquisition of the photos was completed during a particularly bright time of the day, avoiding shadow zones.

### 3.2. Photogrammetric Reconstruction and Structural Analysis

ShapeMetriX 3D software was used for the 3D model reconstruction and structural analysis. The reconstruction of the 3D model was accomplished using 164 frames acquired by means of the SMX—a multi-photo tool based on the structure from motion (SfM) approach. Such a tool allows position reconstruction of every single frame (Image Alignment), and a coarse point cloud—first and a dense point cloud subsequently are obtained. In order to georeference the model, GPS coordinates of specific ground control points (GCPs) were calculated, and the absolute coordinates (WGS84 system) were assigned to each point of the cloud using the SMX-Reference tool implemented in ShapeMetriX 3D.

Once the georeferenced 3D model was obtained, the structural and geo-mechanical analysis of the slope was carried out using the JMS-Analyst tool. This software allows making geometric measurements directly into the 3D model. Each recognized feature can be analyzed using trace measurements by means of trace mode. A trace measurement is a polygonal line that follows the surface of the object in a 3D space. Its length is given along the surface in terms of Euclidean distance. Traces are also used to determine the spacing of a set of structures. The analyst function of the software allows the grouping of the measurements into sets, with automatic clustering and stereographic/statistical projections. Annotations like the length of the drawn track, the dip and dip direction values and the position in terms of X, Y, Z are automatically grouped within the identified discontinuity sets (DS). Thus, the analysis provides clusters representing different sets of rock mass discontinuities. This method is semi-automatic with the possibility of validation. Clustering analysis is used to automatically group the measured discontinuities into DS. It is based on a fuzzy K-means algorithm [47] that aims at minimizing the distance measurements between the average values of the structure sets and the individual measurements. A fuzzy K-means algorithm requires a predefined number of clusters in which the data set must be grouped. Based on current distance measurements, it repeatedly recalculates the mean orientations and groups the data set. An optimal partitioning criterion is applied to judge the optimal number of clusters. Good clustering quality is verified using the following approaches:

- Fuzzy hypervolume (min): clusters must occupy a minimum parameter space. The value must be minimum;
- Average partition density (max): poles must be well concentrated around the set average orientation. The value must be maximum;
- Partition density (max): poles must be well concentrated around the set average orientation. The value must be maximum;

- Xie–Beni index (min): it tests the overall compactness and separation of the poles. The value must be minimum;
- Fukuyama–Sugeno index (min): it correlates the values of the fuzzy cluster objective function to the “cost” of increasing the number of clusters. The value must be minimum.

### 3.3. Kinematic Analysis and Rockfall Susceptibility

Data obtained from structural analysis were used as a basis for a Markland test [48] oriented to the definition of the stability characteristics of the slope in terms of detachment potential. In this perspective, the four DSs identified by means of the clustering analysis were considered, as well as the slope face oriented toward WSW (Dip-Direction 260°) characterized by a slope of 80°. A friction angle of 35° was considered for materials forming the slope. Analysis of the angular relationships between discontinuities and slope surface [49] identified the potential modes of failures, among which are wedge-sliding, planar sliding and non-flexural toppling.

The hazard analysis of a slope can be evaluated with several models based on empirical considerations and assumptions on the slope geometry. In this work, the QPROTO plugin, implemented in Qgis [29], was used. QPROTO allows identifying the most exposed areas to the rock fall phenomenon, taking into account only the slope topography and some empirical parameters. It is based on the cone fall method [50], which enables to quantitatively estimate blocks' velocity and kinetic energy. In QPROTO, a visibility cone is created by identifying all the points of the topographic surface. Visibility cone development starts from the point where an observer is located, which represents the apex of a visibility cone, and the line that joins it with the furthest stop point reached by the falling block (energy line). Its extension is linked to three fundamental angles: inclination, opening and orientation. It is defined as the line joining the source point with the furthest stop point reached by the falling block. Its inclination, expressed as  $\varphi_p(\gamma)$ , defines the energy loss suffered by a boulder and therefore expresses the equivalent boulder-to-slope friction angle [50].

A digital terrain model (DTM) and a shapefile containing the detachment points are needed to run the QPROTO simulation. For each point, the elevation, aspect, propensity to detachment index, block mass, energy line angle, lateral spreading angle and visibility distance must be defined. These parameters were assigned according to the geomechanical analysis. In detail, the detachment index was assigned according to the geomechanical analysis and, subsequently, to the discontinuities' distribution and field observations. Averaging of the most exposed blocks bounded by discontinuities by means of the ShapeMetriX software allowed to assign the block mass volume, while the energy line angle was fixed at 30° after campaign observations of previous falls' blocks.

## 4. Results

### 4.1. Point Clouds and Structural Feature of the Slope

Processing of the acquired 164 frames allowed the creation of the 3D model of the western side of the Cumae Mount. Specifically, a coarse point cloud consisting of approximately 41,300 points and a dense cloud of approximately 1,700,000 points were generated (see a dense cloud in Figure 4a). A visual inspection of the dense point cloud suggests the absence of sparse points and only a few gaps due to the presence of vegetation. The geomechanical analysis derived by the dense point cloud highlight the presence of a total of 118 discontinuities (Figure 4b).

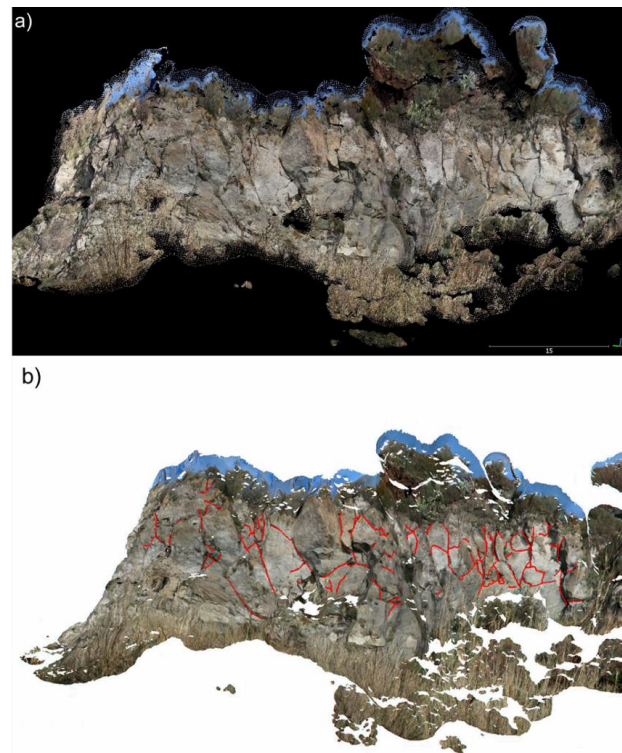


**Figure 4.** (a) Dense point cloud derived by ground-based image processing. (b) Discontinuities are identified within the dense point cloud.

Starting from this data, automatic clustering of discontinuities (CD) was implemented using the algorithms described in Section 3.3, all based on the fuzzy K-means approach [47]. CDs 2 to 4 were hypothesized, clustering was implemented, and analyses carried on. For each analysis, the software-estimated value was compared with the obtained result in order to identify the best, according to a convergence maximization criterion. Cluster analysis quality parameters are reported in Table 1. The conducted analysis shows that the values of the validity indexes are different according to the considered sets. In detail, on the basis of the traced discontinuities, the best results for a good cluster quality forecast are fuzzy hypervolume equal to 0.344, an average partition density equal to 102,408, partition density equal to 100,545, a Xie–Beni index equal to 0.129 and a Fukuyama–Sugeno index equal to  $-23.306$ . Table 1 indicates that for all the considered CDs (CD2, CD3 and CD4), these values show little variations when compared to the best results. In fact, for CD2, there is maximum convergence only for the fuzzy hypervolume index (0.344). Differently, as far as CD3 is concerned, even if the values are similar, there is no convergence. Therefore, the CD was chosen, as 4 indexes out of 5 found perfect convergence and affected Xie–Beni index (0.129), Fukuyama–Sugeno index ( $-23.306$ ), partition density (100.55), and average partition density (102.413). The fuzzy hypervolume index, on the other hand, is 0.369, very close to the Best Results (0.344).

**Table 1.** Quality indexes of the cluster analysis for each considered set (CD2, CD3 and CD4). Bold text indicates full convergence with the best results belonging to the CD4.

Cluster Quality	Best Results	CD2	CD3	CD4
Fuzzy hypervolume	0.344	0.344	0.354	0.369
Average partition density	102.408	98.067	98.761	<b>102.413</b>
Partition density	100.545	95.789	94.757	<b>100.55</b>
Xie–Beni index	0.129	0.229	0.166	<b>0.129</b>
Fukuyama–Sugeno index	$-23.306$	$-9.835$	$-16.564$	<b><math>-23.306</math></b>



From sets of homogeneous discontinuities, DSs were identified, and their geometries in terms of dip-direction and dip-angle are shown in Table 2. The values identified for dip-direction vary from  $11.40^\circ$  (DS4) to  $260.48^\circ$  (DS2) while the dip-angle varies between  $37.84^\circ$  (DS2) and  $74.88^\circ$  (DS1). Figure 5 shows the four identified DSs (Figure 5a) and the polar diagram of the discontinuity rotations (Figure 5b). In particular, green artworks depict the DS1 characterized by 28 discontinuities; magenta artworks represent the DS2 with a total of 21 discontinuities, blue artworks depict the DS3 with a total of 36 discontinuities and cyan artworks represent the DS4 with a total of 33 discontinuities. After average discontinuity attitude was derived by means of clustering analysis. Figure 6 provides an overview of spacing estimation for each of the identified discontinuity sets.

**Table 2.** Discontinuity sets identified through the clustering analysis of discontinuities.

Discontinuity Set	Dip Direction ( $^\circ$ )	Dip ( $^\circ$ )
1	86	75
2	260	37
3	166	62
4	11	66

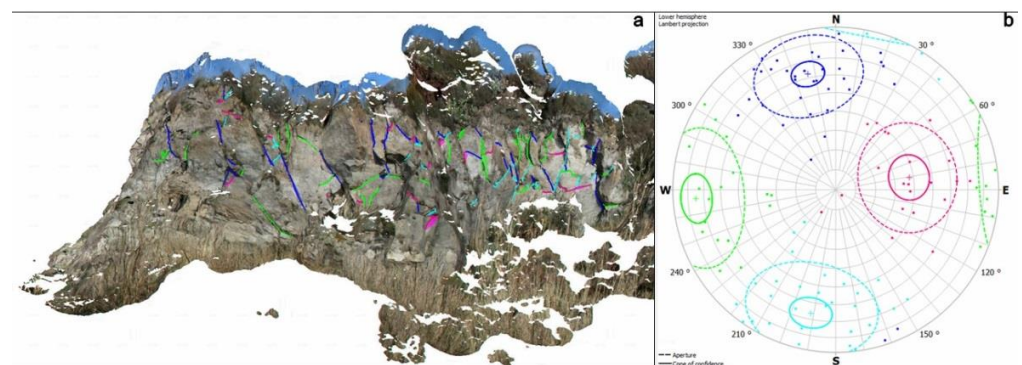


**Figure 5.** (a) Discontinuity sets identified through clustering analysis: green, magenta, blue and cyan artworks represent the discontinuity sets 1, 2, 3 and 4, respectively. (b) Polar diagram showing cluster analysis results.

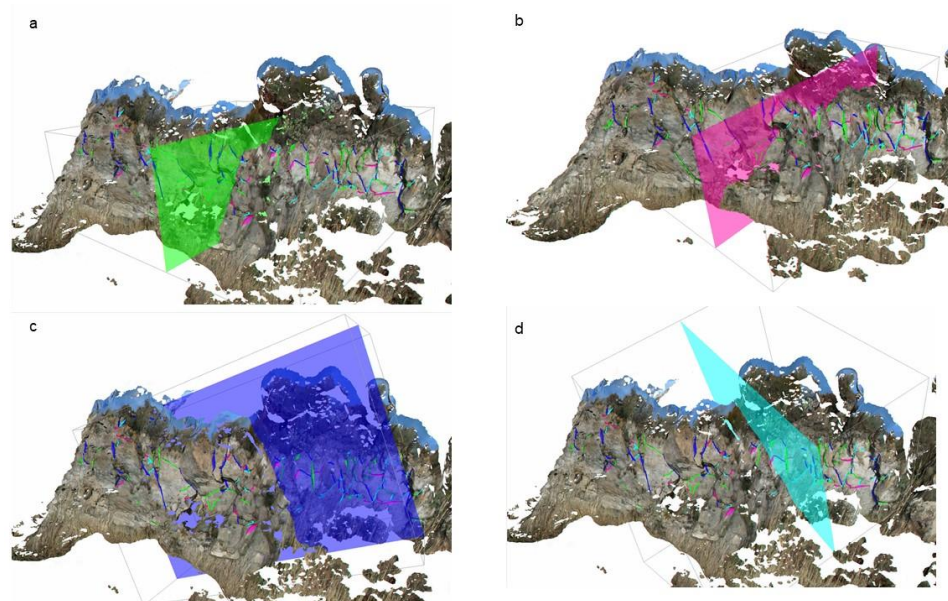


**Figure 6.** Projection plan of discontinuity sets. (a–d) are, respectively, the projection plans of the DSs 1, 2, 3 and 4.

#### 4.2. Kinematic Analysis and Rockfall Susceptibility

Figure 7 shows the results from the Markland test, which points out the potential of block detachment and identifies possible kinematics that can occur in the study area. In detail, the DS1 plane and slope intersection, which falls within the friction angle slope area, indicates a condition of incipient instability for toppling, as shown by the green symbol T1. Moreover, the DS3 plane is parallel to the slope face with an angle of less than  $20^\circ$ , thus creating conditions for planar instability, as shown by the blue symbol P1. Finally, the intersection of DS2 and DS3, falling within the critical area for wedge failure, shows the potential of this kind of instability (i.e., magenta symbol W1).

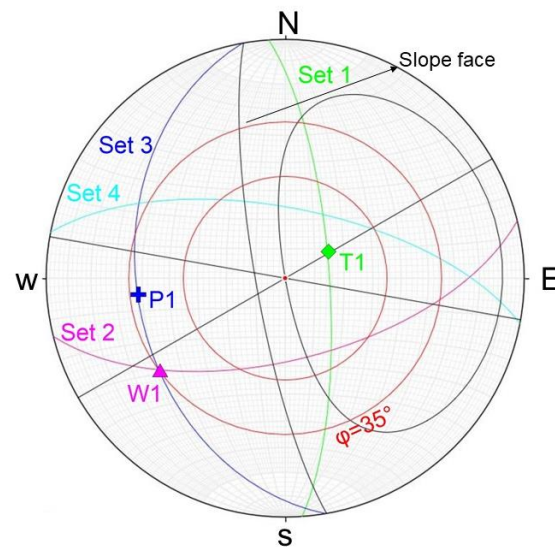


**Figure 7.** Markland test stereographic projections. Discontinuity sets are reported using green, magenta, blue and cyan artworks. Large and small red circles represent the friction angle ( $\varphi = 35^\circ$ ) plane and pole, respectively. Slope face (260/85) and slope direction limits are reported using black lines. The green-diamond T1 indicates the toppling instability, the blue cross P1 identifies the planar break, and the magenta triangle defines wedge break W1.

Results from structural analysis and site surveys allowed us to set all the input parameters necessary for the QPROTO plugin simulations. In detail, the distribution of the recorded fractures enabled the classification of the slope into three sectors with low, medium and high levels of susceptibility to detachment (Figure 8a). Therefore, every above-mentioned sector was given a value of propensity to detachment equal to 0.5, 0.75 and 1, respectively, for increasing susceptibility values. The energy line was evaluated empirically and set at  $30^\circ$ , constant for the entire slope, based on field evidence (fall event occurred in August 2019). As far as block weight is concerned, both the analyses carried out using ShapeMetriX 3D and the blocks at the toe of the slope were considered. A weight of about 1500 kg, corresponding to approximately  $0.5 \text{ m}^3$ , was therefore estimated. The energy angle value was set at  $15^\circ$ , as suggested by the authors of the plugin [29]. Finally, the elevation value was extracted from the digital terrain model (LIDAR with  $1 \text{ m} \times 1 \text{ m}$  resolution) used for the analysis (<http://sit.cittametropolitana.na.it/lidar.html>). The results are shown in Figure 8b, in terms of the level of susceptibility. It is possible to notice a sort of linear relationship between the propensity to detach and the susceptibility to run out. In fact, starting from the northern sector, where the propensity to detach is limited (low value), a very low susceptibility to run out can be seen. Differently, in the central sector, the average detachment propensity corresponds to a susceptibility that varies from limited to medium. The highest levels of susceptibility, on the other hand, were recorded in the southern sector, where the propensity to break away is the highest one. It is noteworthy that the highest obtained susceptibility value corresponded to the site affected by the recent

fall that occurred in August 2019. Thus, the studied area shows a high level of risk as the detected susceptibility interacts with both the Cumana station and the railroad.

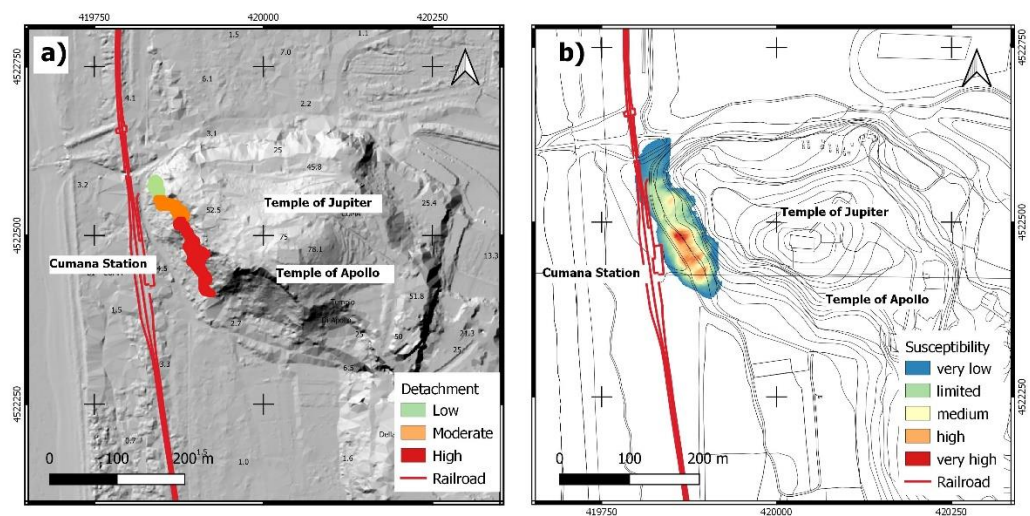


**Figure 8.** (a) Slope sectors detachment probability map. (b) Susceptibility to rockfall.

## 5. Discussion and Conclusions

The Italian territory is scattered with important archaeological sites, 51 of which have been identified as UNESCO heritage sites. Such sites are evidence of civilizations and the history of peoples, and they represent an important cultural heritage that is increasingly valorized by specific financial measures. Across the National territory, such sites are often subject to hazardous geological processes such as landslides, earthquakes and floods that threaten them, making their fruition and preservation very challenging tasks [51–54]. In this condition, while susceptibility and hazard analyses form a substantial basis for site management and process mitigation, real-time monitoring of sites is of great importance for safer fruition by the visitors. The use of innovative monitoring technologies, such as satellite-based observation and low-cost sensors [55,56], together with conventional techniques, have proved to be valid tools for the detection of ongoing hazardous processes that threaten cultural heritage. Some examples of these procedures are the geotechnical characterization of limestones employed in the reconstruction of Saint Nicholas Cathedral, a UNESCO World Heritage monument in south-eastern Sicily [57] and monitoring by means of Internet-of-Things (IoT) techniques carried out in the city of Matera, the European capital of culture in 2019 [58]. In the first case, the objective was to investigate the mechanical features of the materials used for a specific building (Cathedral) in order to evaluate their degree of alteration and, therefore, indicate the interventions to be implemented for conservation. In the second case, the study focused on the implementation of a large-scale monitoring system by means of an IoT approach, which proved to be useful for the conservation of the Matera city center.

Archaeological sites fruition and conservation issues related to natural hazards highlight the need for a better knowledge of active processes and their potential future evolution. In this perspective, the knowledge of the process is a first step toward the potential definition of mitigation strategies that may contribute to the long-term fruition of the site in a safer manner.

Cumae is one of the most important archaeological sites in Italy, with several thousands of visitors every year. Its historical importance and the risk for visitors to be exposed to rockfall, which may compromise its fruition, make this site particularly significant. In this context, the occurrence of rockfall along the access course, located within the forest of Cuma, which represents a further element of cultural value for the park, is a major issue from a safety management perspective. Therefore, specific analyses are required to guide planning measures.

Specifically, digital terrestrial photogrammetry, adopted for the survey of the area, allowed the identification of 118 discontinuities, which were clustered into four discontinuity sets. The Markland Test, completed on the basis of clustered data, confirmed the potential of slope instability at the site in the form of toppling, wedge and planar slides. A better definition of the behavior of potentially unstable blocks was achieved by means of a susceptibility analysis carried out using QPROTO Plugin and observation-based parameterization. As a result, the sector with high susceptibility was identified as the one corresponding to the segment of the access course adjacent to the railroad station. Overall, this study provided a qualitative estimation of rockfall susceptibility in an area characterized by limited access, as well as obtaining a product able to support the development of a management plan oriented to increased safety in the site in fruition perspective. This is particularly important considering that the Cumae Archeological Site includes unique elements of very high cultural value, such as the Cumaean Sybil's Cave, the Roman crypt, the temples of Jupiter and Apollo and the lower city. Even if rockfall related risk is the most evident, recent archaeological research have shown that archaeological ruins, such as a burial chamber, were reburied probably because of the deterioration of the local drainage channel system, suggesting the potential for additional hazardous processes [38,56]. Moreover, the subsidence and rising of the water table led to the flooding of +1.20 m above the archaeological remains, creating structural damage and decay of decorative elements.

This study is part of a larger project that includes surveys and monitoring of the whole area of the archaeological site. To this purpose, the most advanced technologies will be used for the survey and monitoring of natural phenomena affecting the site. Actually, three-dimensional survey techniques will be employed using terrestrial laser scanners and unmanned aerial vehicles in order to implement three-dimensional models (point clouds) useful for studying the stability of the fronts of the Roman crypt and the Cumaean Sybil's Cave, already subject to mitigation measures in the past. On the other hand, the phenomenon of subsidence, which affects the lower town, will be investigated by means of differential interferometry SAR (DInSAR) techniques. This technique allows the estimation of terrain deformations with subcentimetric accuracy and has been widely used in archaeological areas [52,53]. The integration of these techniques will allow better fruition of the site, ensuring, on one hand, the safety of visitors and, on the other hand, the enhancement and preservation of archaeological remains.

**Author Contributions:** Conceptualization, L.R. and D.D.M.; methodology, R.D.S., D.I.; software, R.D.S., D.D.M. and L.G.; validation, L.G. and L.R.; resources, F.P.; data curation, R.D.S., D.D.M. and L.G.; writing—original draft preparation, R.D.S., L.G., L.R.; writing—review and editing, D.I. and V.M.; supervision, V.M., D.D.M. All authors have read and agreed to the published version of the manuscript.

**Funding:** This research was partially funded by AIM Project, grant number AIM18352321-1.

**Institutional Review Board Statement:** Not applicable.

**Informed Consent Statement:** Informed consent was obtained from all subjects involved in the study.

**Data Availability Statement:** The data presented in this study are available on request to the corresponding author.

**Acknowledgments:** The authors thank Consorzio interUniversitario per la prevenzione dei Grandi Rischi (CUGRI) for providing technological support. In addition, the authors would like to thank the three anonymous reviewers for their valuable and insightful comments to improve the paper.

**Conflicts of Interest:** The authors declare no conflict of interest.

## References

1. Farella, E.; Menna, F.; Nocerino, E.; Morabito, D.; Remondino, F.; Campi, M. Knowledge and valorization of historical sites through 3d documentation and modeling. *Int. Arch. Photogramm. Remote Sens. Spat. Inf. Sci.* **2016**, *41*, 255–262. [[CrossRef](#)]
2. Incoronato, L. The Archaeological and Natural Park of Cuma in the Phlegraean Fields: A planning proposal. *UPLanD-J. Urban Plan. Landsc. Environ. Des.* **2019**, *4*, 17–28.

3. D'Agostino, B.; Fratta, F.; Malpede, V. *Cuma. Le Fortificazioni*; L'Orientale Università degli Studi: Napoli, Italy, 2005.
4. Caputo, P.; Morichi, R.; Paone, R.; Rispoli, P. *Cuma e il Suo Parco Archeologico, un Territorio e le Sue Testimonianze*; Scienze e Lettere: Roma, Italy, 2010.
5. Pagano, M. L'acropoli di Cuma e l'antro della Sibilla. M. GIGANTE (a cura di). *Civ. Campi Flegrei* **1992**, *8*, 261–330.
6. Di Napoli, M.; Marsiglia, P.; Di Martire, D.; Ramondini, M.; Ullo, S.L.; Calcaterra, D. Landslide susceptibility assessment of wildfire burnt areas through earth-observation techniques and a machine learning-based approach. *Remote Sens.* **2020**, *12*, 2505. [[CrossRef](#)]
7. Matano, F. Analysis and classification of natural and human-induced ground deformations at regional scale (Campania, Italy) detected by satellite synthetic-aperture radar interferometry archive datasets. *Remote Sens.* **2019**, *11*, 2822.
8. Di Martire, D.; De Rosa, M.; Pesce, V.; Santangelo, M.A.; Calcaterra, D. Landslide hazard and land management in high-density urban areas of Campania region, Italy. *Nat. Hazards Earth Syst. Sci.* **2012**, *12*, 905–926. [[CrossRef](#)]
9. Morra, V.; Calcaterra, D.; Cappelletti, P.; Colella, A.; Fedele, L.; de' Gennaro, R.; Langella, A.; Mercurio, M.; de' Gennaro, M. Urban geology: Relationships between geological setting and architectural heritage of the Neapolitan area. *J. Virtual Explor.* **2010**, *36*, 26. [[CrossRef](#)]
10. Finicelli, G.F.; Confuorto, P.; Carratù, M.T.; Di Martire, D. Multivariate Statistical approach vs. Deterministic physically based model for landslide susceptibility assessment. *Rend. Online Soc. Geol. It.* **2016**, *41*, 151–154. [[CrossRef](#)]
11. Carotenuto, F.; Angrisani, A.C.; Bakthiari, A.; Carrat, M.T.; Di Martire, D.; Finicelli, G.F.; Raia, P.; Calcaterra, D. A New Statistical Approach for Landslide Susceptibility Assessment in the Urban Area of Napoli (Italy). In *Advancing Culture of Living with Landslides*; Springer International Publishing AG: Cham, Switzerland, 2017; pp. 881–889. [[CrossRef](#)]
12. Calcaterra, D.; Del Prete, S.; Mele, R. The influence of landslides on the coastal settlements of the Phlegrean district (Campania region, Italy). In Proceedings of the Internet Conference CITTAM 2003 "The Requalification of Mediterranean Coasts among Tradition, Development and Sustainability", Naples, Italy, 26–28 June 2003; pp. 524–534. (In Italian).
13. Calcaterra, D.; de Riso, R.; Nave, A.; Sgambati, D. The role of historical information in landslide hazard assessment of urban areas: The case of Naples (Italy). In Proceedings of the 1st European Conference on Landslides, Prague, Czech Republic, 24–26 June 2002; pp. 129–135.
14. Calcaterra, D.; Guarino, P.M. Morphodynamics and recent landslides in the Neapolitan slopes (western sector). *Geol. Tec. Ambient.* **1999**, *2*, 11–17. (In Italian)
15. Calcaterra, D.; Guarino, P.M. Recent landslides in the urban area of Naples: The middle-eastern sector. In Proceedings of the Conference on "Geologia delle Grandi Aree Urbane", Bologna, Italy, 4–5 November 1997; pp. 257–261. (In Italian).
16. Parise, M.; Calcaterra, D.; de Luca Tupputi Schinosa, F.; Palma, B. Rockfall stability assessment at the western slope of Camaldoli Hill (Naples, Italy). In Proceedings of the 9th Internet Symposium on Landslides, Rio de Janeiro, Brazil, 28 June–2 July 2004; Volume 28. [[CrossRef](#)]
17. Corominas, J.; van Westen, C.; Frattini, P.; Cascini, L.; Malet, J.P.; Fotopoulou, S.; Catani, F.; Van Den Eeckhaut, M.; Mavrouli, O.; Agliardi, F.; et al. Recommendations for the quantitative analysis of landslide risk. *Bull. Eng. Geol. Environ.* **2014**, *73*, 209–263. [[CrossRef](#)]
18. Frattini, P.; Crosta, G.; Carrara, A.; Agliardi, F. Assessment of rockfall susceptibility by integrating statistical and physically-based approaches. *Geomorphology* **2008**, *94*, 419–437. [[CrossRef](#)]
19. Guzzetti, F.; Reichenbach, P.; Wiecek, G.F. Rockfall hazard and risk assessment in the Yosemite Valley, CA, USA. *NHESS* **2003**, *3*, 491–503.
20. Messenzehl, K.; Meyer, H.; Otto, J.C.; Hoffmann, T.; Dikau, R. Regional-scale controls on the spatial activity of rockfalls (Turtmann Valley, Swiss Alps)—A multivariate modeling approach. *Geomorphology* **2016**, *287*, 29–45. [[CrossRef](#)]
21. Samodra, G.; Chen, G.; Sartohadi, J.; Hadmoko, D.S.; Kasama, K.; Setiawan, M.A. Rockfall susceptibility zoning based on back analysis of rockfall deposit inventory in Gunung Kelir, Java. *Landslides* **2016**, *13*, 805–819. [[CrossRef](#)]
22. Matasci, B.; Stock, G.M.; Jaboyedoff, M.; Carrea, D.; Collins, B.D.; Guérin, A.; Matasci, G.; Ravelin, L. Assessing rockfall susceptibility in steep and overhanging slopes using three-dimensional analysis of failure mechanisms. *Landslides* **2018**, *15*, 859–878. [[CrossRef](#)]
23. Rodriguez, J.; Macciotta, R.; Hendry, M.T.; Roustaei, M.; Gräpel, C.; Skirrow, R. UAVs for monitoring, investigation, and mitigation design of a rock slope with multiple failure mechanisms—A case study. *Landslides* **2020**. [[CrossRef](#)]
24. Francioni, M.; Antonaci, F.; Sciarra, N.; Robiati, C.; Coggan, J.; Stead, D.; Calamita, F. Application of unmanned aerial vehicle data and discrete fracture network models for improved rockfall simulations. *Remote Sens.* **2020**, *12*, 2053. [[CrossRef](#)]
25. Riquelme, A.; Tomás, R.; Cano, M.; Pastor, J.L.; Abellán, A. Automatic mapping of discontinuity persistence on rock masses using 3D point clouds. *Rock Mech. Rock Eng.* **2018**, *51*, 3005–3028. [[CrossRef](#)]
26. Riquelme, A.J.; Abellán, A.; Tomás, R. Discontinuity spacing analysis in rock masses using 3D point clouds. *Eng. Geol.* **2015**, *195*, 185–195. [[CrossRef](#)]
27. Mineo, S.; Pappalardo, G. Sustainable fruition of cultural heritage in areas affected by rockfalls. *Sustainability* **2020**, *12*, 296. [[CrossRef](#)]
28. Pappalardo, G.; Imposa, S.; Mineo, S.; Grassi, S. Evaluation of the stability of a rock cliff by means of geophysical and geomechanical surveys in a cultural heritage site (south-eastern Sicily). *Ital. J. Geosci.* **2016**, *135*, 308–323. [[CrossRef](#)]
29. Castelli, M.; Grisolia, M.; Barbero, M.; Vallerio, G.; Campus, S.; Rocco Pispico, R.; Lanteri, L. QPROTO—A QGIS plugin for rockfall analyses at small scale. In *DISEG Politecnico di Torino*; Politecnico di Torino: Turin, Italy, 2016; pp. 1–36.

30. Sacchi, M.; Passaro, S.; Molisso, F.; Matano, F.; Steinmann, L.; Spiess, V.; Pepe, F.; Corradino, M.; Caccavale, M.; Tamburrino, S.; et al. The holocene marine record of unrest, volcanism, and hydrothermal activity of Campi Flegrei and Somma-Vesuvius. *Vesuvius Campi Flegrei Campanian Volcanism* **2020**, 435–469. [[CrossRef](#)]
31. De Vivo, B.; Rolandi, G.; Gans, P.B.; Calvert, A.; Bohron, W.A.; Spera, F.J.; Belkin, H.E. New constraints on the pyroclastic eruptive history of the Campanian volcanic Plain (Italy). *Mineral. Petrol.* **2001**, *73*, 47–65. [[CrossRef](#)]
32. Fedele, L.; Scarpati, C.; Lanphere, M.; Melluso, L.; Morra, V.; Perrotta, A.; Ricci, G. The Breccia Museo formation, Campi Flegrei, southern Italy: Geochronology, chemostratigraphy and relationship with the Campanian Ignimbrite eruption. *Bull. Volcanol.* **2008**, *70*, 1189–1219. [[CrossRef](#)]
33. Deino, A.L.; Orsi, G.; de Vita, S.; Piochi, M. L'età dell'eruzione caldera napoletana di tufo giallo (caldera dei Campi Flegrei—Italia) valutata con il metodo di datazione  $^{40}\text{Ar}/^{39}\text{Ar}$ . *J. Volcanol. Geotherm. Res.* **2004**, *133*, 157–170.
34. Perrotta, A.; Scarpati, C.; Luongo, G.; Morra, V. The Campi Flegrei caldera boundary in the city of Naples. *Chapter 5 Dev. Volcanol.* **2006**, *9*, 85–96. [[CrossRef](#)]
35. Melluso, L.; de Gennaro, R.; Fedele, L.; Franciosi, L.; Morra, V. Evidence of crystallization in residual, Cl–F-rich, agpaite, trachyphonolitic magmas and primitive Mg-rich basalt–trachyphonolite interaction in the lava domes of the Phlegrean Fields (Italy). *Geol. Mag.* **2012**, *149*, 532–550. [[CrossRef](#)]
36. Allocca, V.; Coda, S.; De Vita, P.; Di Rienzo, B.; Ferrara, L.; Giarra, A.; Mangoni, O.; Stellato, L.; Trifuoggi, M.; Arienzo, M. Hydrogeological and hydrogeochemical study of a volcanic-sedimentary coastal aquifer in the archaeological site of Cumae (Phlegraean Fields, southern Italy). *J. Geochem. Explor.* **2018**, *185*, 105–115. [[CrossRef](#)]
37. Lirer, L.; Petrosino, P.; Alberico, I.; Armiero, V. Cartografia. In *I Campi Flegrei: Storia di un campo vulcanico. Quaderni dell'Accademia Pontaniana*; Lirer, L., Ed.; Accademia Pontaniana-Giannini: Napoli, Italy, 2011; ISBN 9788874315147.
38. Vitale, S.; Isaia, R. Fractures and faults in volcanic rocks (Campi Flegrei, southern Italy): Insight into volcano-tectonic processes. *Int. J. Earth Sci.* **2014**, *103*, 801–819. [[CrossRef](#)]
39. Bravi, S.; Fuscaldo, M.; Guarino, P.M.; Schiattarella, M. Evoluzione sedimentaria olocenica dell'area dell'antico Porto di Cumae (Campi Flegrei, Italia meridionale). In *Variazioni Climatico-Ambientali ed Impatto Sull'uomo Nell'area Circum-Mediterranea Durante l'Olocene*; Livadie, C.A., Ortolani, F., Eds.; Territorio Storico e Ambiente Edition; EdiPuglia: Bari, Italy, 2003; pp. 23–64.
40. Sturzenegger, M.; Stead, D. Close-range terrestrial digital photogrammetry and terrestrial laser scanning for discontinuity characterization on rock cuts. *Eng. Geol.* **2009**, *106*, 163–182. [[CrossRef](#)]
41. Krosley, L.; Oerter, E.; Ortiz, T.; Ortiz, T. Digital ground-based photogrammetry for measuring discontinuity orientations in steep rock exposures. In *Golden Rocks 2006, Proceedings of the 41st US Symposium on Rock Mechanics (USRMS), Golden, CO, USA, June 2006*; American Rock Mechanics Association: Edinburgh, UK, 2006.
42. Pappalardo, G.; Mineo, S.; Rapisarda, F. Rockfall hazard assessment along a road on the Peloritani Mountains (northeastern Sicily, Italy). *Nat. Hazards Earth Syst. Sci.* **2014**, *14*, 2735–2748.
43. Francioni, M.; Stead, D.; Sciarra, N.; Calamita, F. A new approach for defining Slope Mass Rating in heterogeneous sedimentary rocks using a combined remote sensing GIS approach. *Bull. Eng. Geol. Environ.* **2019**, *78*, 4253–4274. [[CrossRef](#)]
44. Haneberg, W.C. Elevation errors in a LiDAR digital elevation model of West Seattle and their effects on slope stability calculations. *Rev. Eng. Geol.* **2008**, *20*, 55–65.
45. Galantucci, R.A.; Fatiguso, F. Advanced damage detection techniques in historical buildings using digital photogrammetry and 3D surface analysis. *J. Cult. Herit.* **2019**, *36*, 51–62. [[CrossRef](#)]
46. Westoby, M.J.; Brasington, J.; Glasser, N.F.; Hambrey, M.J.; Reynolds, J.M. 'Structure-from-Motion' photogrammetry: A low-cost, effective tool for geoscience applications. *Geomorphology* **2012**, *179*, 300–314. [[CrossRef](#)]
47. Hammah, R.E.; Curran, J.H. Fuzzy cluster algorithm for the automatic identification of joint sets. *Int. J. Rock Mech. Min. Sci.* **1998**, *35*, 889–905.
48. Markland, J.T. *A Useful Technique for Estimating the Stability of Rock Slopes When the Rigid Wedge Sliding Type of Failure Is Expected*; Imp. Coll. Rock Mech. Res. Rep. 19; Imperial College of Science and Technology: London, UK, 1972.
49. Kliche, C.A. Rock slope stability. In *Society for Mining, Metallurgy, and Exploration*; SME: Littleton, CO, USA, 1999.
50. Jaboyedoff, M.; Labiouse, V. Preliminary estimation of rockfall runoff zones. *Nat. Hazards Earth Syst. Sci.* **2011**, *11*, 819. [[CrossRef](#)]
51. Rispoli, C.; Di Martire, D.; Calcaterra, D.; Cappelletti, P.; Graziano, S.F.; Guerriero, L. Sinkholes threatening places of worship in the historic center of Naples. *J. Cult. Herit.* **2020**. [[CrossRef](#)]
52. Cigna, F.; Confuorto, P.; Novellino, A.; Tapete, D.; Di Martire, D.; Ramondini, M.; Calcaterra, D.; Plank, S.; Ietto, F.; Brigante, A.; et al. 25 years of satellite InSAR monitoring of ground instability and coastal geohazards in the archaeological site of Capo Colonna, Italy. In *Proceeding SPIE 10003, SAR Image Analysis, Modeling, and Techniques XVI*; International Society for Optics and Photonics: Bellingham, WA, USA, 2016. [[CrossRef](#)]
53. Bianchini, S.; Moretti, S. Analysis of recent ground subsidence in the Sibari plain (Italy) by means of satellite SAR interferometry-based methods. *Int. J. Remote Sens.* **2015**, *18*, 4550–4569. [[CrossRef](#)]
54. Stellato, L.; Coda, S.; Arienzo, M.; De Vita, P.; Di Rienzo, B.; D'Onofrio, A.; Ferrara, L.; Marzaioli, F.; Trifuoggi, M.; Allocca, V. Natural and anthropogenic groundwater contamination in a coastal volcanic sedimentary aquifer: The case of the archaeological site of Cumae (Phlegraean Fields, Southern Italy). *Water* **2020**, *12*, 3463.
55. Guerriero, L.; Guerriero, G.; Grelle, G.; Guadagno, F.M.; Revellino, P. Brief Communication: A low-cost Arduino<sup>®</sup>-based wire extensometer for earth flow monitoring. *Nat. Hazards Earth Syst. Sci.* **2017**, *17*, 881. [[CrossRef](#)]

- 
56. Ruzza, G.; Guerriero, L.; Revellino, P.; Guadagno, F.M. A Multi-Module Fixed Inclinometer for Continuous Monitoring of Landslides: Design, Development, and Laboratory Testing. *Sensors* **2020**, *20*, 3318. [[CrossRef](#)] [[PubMed](#)]
  57. Pappalardo, G.; Mineo, S.; Monaco, C. Geotechnical characterization of limestones employed for the reconstruction of a UNESCO world heritage Baroque monument in southeastern Sicily (Italy). *Eng. Geol.* **2016**, *212*, 86–97. [[CrossRef](#)]
  58. Gribaudo, M.; Iacono, M.; Levis, A.H. An IoT-based monitoring approach for cultural heritage sites: The Matera case. *Concurr. Comput. Pract. Exp.* **2017**, *29*, e4153. [[CrossRef](#)]